Journal of Power Sources 206 (2012) 325–333

Contents lists available at SciVerse ScienceDirect

Journal of Power Sources

journal homepage: www.elsevier.com/locate/jpowsour

Nano SiO_2 particle formation and deposition on polypropylene separators for lithium-ion batteries

Dong Fu [a], Ben Luan [a,*], Steve Argue [b], Martin N. Bureau [c], Isobel J. Davidson [b]

[a] Center for Automotive Materials Manufacturing, Industrial Materials Institute, National Research Council Canada, 800 Collip Circle, London, Ontario N6G 4X8, Canada
[b] Institute for Chemical Process and Environmental Technology, National Research Council Canada, 1200 Montreal Road Building M-12, Ottawa, Ontario K1A 0R6, Canada
[c] Industrial Materials Institute, National Research Council Canada, 75 de Mortagne Boulevard, Boucherville, Quebec J4B 6Y4, Canada

ARTICLE INFO

Article history:
Received 7 October 2011
Received in revised form 27 October 2011
Accepted 31 October 2011
Available online 6 November 2011

Keywords:
Lithium-ion batteries
Separators
Silica coating
Rate capability
Thermal shrinkage

ABSTRACT

The novelty of this work is the formation and deposition of SiO_2, as opposed to deposition using commercially available SiO_2 powder suspension in the solution, to form ceramic coating on polypropylene (PP) separators for lithium-ion battery. The formation of SiO_2 nanoparticles with uniform particle size is accomplished through direct hydrolysis of tetraethyl orthosilicate (TEOS), while the deposition of the formed SiO_2 on PP separators was conducted in the same solution containing polyvinylidene fluoride-hexafluoropropylene (PVDF-HFP) as binders and acetone as the solvent. The effects of the ceramic coating on the surface morphology, tensile strength, contact angles, electrolyte uptake, thermal shrinkage of the PP separators and the cell performances such as battery rate capability and Coulombic efficiency were investigated. The coated separators show significant reduction in thermal shrinkage and improvement in tensile strength, contact angles, electrolyte uptake and battery performance as compared to the plain PP separator.

1. Introduction

Lithium-ion batteries are widely used for electronic devices such as mobile phones, laptop computers, and digital cameras due to their high energy density and long life cycle. With the search for a solution as alternative propulsion system, lithium-ion batteries are also expected to be an alternative power source for Plug-in Hybrid Electric Vehicle (PHEV), particularly with the heightened needs for alternative energy and environment protection, due to the advantages in longer cycle life, higher voltages and energy density when compared with other rechargeable batteries [1–6].

The separator in a battery plays an important role to retain electrolyte, prevent shortage between the two electrodes while maintaining high ion permeation, and to perform safe deactivation of the cell under overcharge, abnormal heating or mechanical rupture conditions [7,8]. In general, separators in lithium-ion batteries are made of polyolefins, predominantly polyethylene (PE) or polypropylene (PP). However, even though these microporous polyolefin based separators have many advantages in terms of added mechanical integrity and the additional advantage of exhibiting thermal shut-down under severe abuse conditions [7], the thermal shrinkage and mechanical strength are still serious concerns over their ability to maintain the necessary electrical isolation between electrodes when considered for higher power output for onboard electric vehicle applications [9]. Another concern is related to the formation of dendrites formed during the charge/discharge cycling of cells which could protrude through the separators and create short circuiting of the electrodes which poses a serious safety concern [10–12].

Recently, various approaches to overcome these shortcomings of polyolefin based separators have been reported. Most reports focused on many alternatives of polyolefin based separators such as non-woven separators and inorganic composite [13–18]. Another recent approach was the coating of polyolefin based separators using inorganic particles due to the excellent thermal stability and wettability of inorganic particles with organic electrolytes. This approach significantly improves the thermal shrinkage and electrochemical performance of the separators [19–26]. However, in these studies, commercially available inorganic powders (such as clay, SiO_2, Al_2O_3, etc.) were suspended in acetone based solutions with polyvinylidene fluoride-hexafluoropropylene (PVdF-HFP) as binders to attach the inorganic particles on the separator surface to form nanocomposite separators. Examples of such nanocomposites are characterized of SiO_2 nanoparticles embedded in a polymer matrix hence the establishment of a highly ordered nanoporous structure, reported by Park and Jeong and Lee [19,26]. The SiO_2 nanoparticles are close-packed and interconnected by organic binders (PVdF-HFP) on both sides of a PE separator. However, the inorganic particles are easy to form aggregates or agglomerates. Consequently, sonication and ball milling had to be used to

* Corresponding author. Tel.: +1 519 430 7043; fax: +1 519 430 7032.
E-mail address: ben.luan@nrc-cnrc.gc.ca (B. Luan).

0378-7753/$ – see front matter
doi:10.1016/j.jpowsour.2011.10.130

distribute the inorganic particles evenly in the solvents to possibly form a uniform solution. However, this treatment represents an added investment and processing. Also, wet ball milling leads to unavoidable usage of higher viscose solutions for higher ball milling efficiency because viscosity appears to have the most significant effect on the rate of particle size reduction [27]. Higher solution viscosity results in thicker than desired coating and consequently the reduction of available space for active materials in the cell and the increase of cell weight, both are detrimental to the specific energy density of batteries [26]. In addition, excessive build up of coating could also clog up the pores in the separator which compromises the ionic conductivity and the electrochemical kinetics.

In this paper, a new process was developed for the coating of separators, featuring synthesis of SiO_2 nanoparticles and its deposition on separators. It ought to be noted that the synthesis of SiO_2 was based on the Stöber method [28,29]. The differences of our work includes: (1) formation of SiO_2 in a different solution. Stöber method used methanol, ethanol, propanol and butanol as solvents, while acetone was used in our work; and (2) Stöber method focused solely on the formation of particles but did not address the deposition of the formed particles. In our work, PVdF-HFP was used as a binder to facilitate the deposition of the formed SiO_2 particles. This new approach of hydrolysis of tetraethyl orthosilicate (TEOS) to form SiO_2 and the deposition on PP membrane separator in PVDF-HFP acetone solution results in the coating of evenly distributed particles of uniform size distribution. All this was accomplished through a simple yet effective immersion of the separator membrane in the solution described above. This process avoided sonication and ball milling for suspension and distribution of the ceramic nanoparticles in the solution. The effects of the ceramic coating on the separator surface morphology, tensile strength, contact angels, electrolyte uptake, thermal shrinkage, the cell charge/discharge Coulombic efficiency, and the significant improvement of battery rate capability were investigated, and compared with those obtained with a plain PP separator without coating.

2. Experimental

2.1. Chemicals and materials

All chemicals were purchased and used as received without further purification or modification. Celgard® 2500 separators were purchased from Celgard Company (25 μm microporous monolayer Polypropylene membrane with a porosity of 55%).

2.2. Coating of separators

Dissolving 1 g of PVdF-HFP (Aldrich) in 160 ml acetone, followed by the addition of 6 ml de-ionized water and 3 ml ammonium hydroxide (30% Fisher scientific) into the solution with vigorous stirring for 20 min. Subsequently, 6 ml of TEOS (Aldrich) was added into the solution followed by a continuous agitation for 5 h until the solution color changed from clear to uniformly cloudy. Both sides of the PP separators can then be coated with a simple immersion of the separator into the prepared solution. The coated separators were then dried at room temperature to evaporate acetone.

2.3. Characterizations of separators

The morphology of the membrane was investigated using a field emission scanning electron microscope (FE-SEM, S-4800, Hitachi). The samples were also analyzed with X-ray photoelectron spectroscopy (XPS) using a Kratos Axis Ultra X-ray photoelectron spectrometer which probes the surface of the sample to a depth of 7–10 nm, and has detection limits ranging from 0.1 to 0.5 atomic percent depending on the elements. The specific surface areas, pore sizes and pore volume were determined using a Micromeritics ASAP 2010 nitrogen adsorption apparatus (Micromeritics, USA). All the samples were degassed at 80 °C prior to measurements. The specific surface area was calculated by the Brunauer–Emmett–Teller (BET) method. The pore size was obtained from the maxima of the pore size distribution curve calculated by the Barrett–Joyner–Halenda (BJH) method using the desorption branch of the isotherm, and the total pore volume was evaluated by the single point method. The thermal shrinkage of the SiO_2 coated separators was determined by measuring the dimensional change after being subjected to heat treatment at various temperatures for 30 min in a temperature chamber (TESTEQUITY 1000 series). The electrolyte uptake (T) of the membrane was determined by immersing the membrane in 1 M $LiPF_6$ (DMC/EC; 1:1 in volume) for 30 min and obtained by:

$$T(\%) = \frac{W_2 - W_1}{W_1} \times 100 \quad (1)$$

where W_1 and W_2 are the mass of the dry and wet membranes, respectively.

The surface advancing contact angles were measured using a contact angle meter (Kernco Instruments, USA). The same electrolyte used for battery assembling, 1 M $LiPF_6$ in DMC/EC (1:1 in volume), was dropped onto the sample using a microsyringe during the test. A picture of the drop was captured after the drop set onto the sample. The contact angles were calculated through analyzing the shape of the drop. The tensile strength of the films was obtained from the recorded load–displacement curve of specimens with a cross section width of 10 mm pulled at a speed of 5 mm min^{-1} mm using a tension machine (INSTRON microtensile, UK) with a 2 kN load cell. The electrochemical properties of the assembled 2325 button style lithium test cells were investigated using a 16 Channel Arbin BT 2043 battery test system. The cathodes of the test cells were prepared by slurry coating a mixture of $LiCoO_2$, Super S carbon, Lonza EKS-4 graphite with a PVDF binder onto high purity aluminum foil which was then dried and pressed. The anode used was high purity lithium metal. The test cells were assembled in a dry, oxygen free glove box using a single layer of the test separators that had been previously dried in a vacuum oven at 40 °C for 12 h. A 35 μl aliquot of 1 M $LiPF_6$ in DMC/EC (1:1) was placed onto the cathode, followed by the test separator that had been wetted with another 35 μl aliquot of the electrolyte in a glass dish before placing. A final 35 μl aliquot of the electrolyte was then added on top of the separator prior to placing the anode and completing the cell build.

3. Results and discussion

TEOS can be easily hydrolyzed to form SiO_2 particles under catalysis of ammonium hydroxide, i.e. Stöber method, as shown in Eq. (2).

$$Si(OC_2H_5)_4 + H_2O \xrightarrow{NH_3} SiO_2 + 4C_2H_5OH \quad (2)$$

The mechanism of Stöber method with respects to silica particle formation, growth, and particle size, distribution, and shape have been investigated in the past decades [30–42]. However, the mechanisms reported by different researchers are contradictory. Wang et al. summarized the mechanisms from literatures which may be sorted into two different models: the monomer addition model and the controlled aggregation model [42]. The monomer addition model argues that after a limited period of time for nucleation, growth occurs through the addition of hydrolyzed monomers to the oligomers surface and gradually becomes the dominant process [30,33,34]. On the contrary, the controlled aggregation model

claims that the aggregation of sub-particles leads to particle formation [31,32,37,40,41]. Recent results reported seems to support the monomer addition model [42].

While the above reaction forms SiO_2 particles, deposition of the formed particles onto the separator surface takes place in the same solution because of the co-existence of PVdF-HFP in the solution, according to our novel electrolyte formulation. Unlike reported by others [19,26], our method provides a simplified process of coating, without having to use costly and time-consuming sonication and ball milling to suspend and distribute the nanoparticles produced by the suppliers. To our knowledge, this synthesis and deposition of SiO_2 nanoparticles in the PVDF-HFP acetone solution for separator coating is reported for the first time. In addition, both the particle size and the uniformity of particle size distribution can be easily controlled by adjusting the synthesis conditions.

XPS survey scan analyses were carried out with an analysis area of 300 μm × 700 μm and a pass energy of 160 eV (Fig. 1(a)). High resolution analyses were carried out with an analysis area of 300 μm × 700 μm and a pass energy of 20 eV. Fig. 1(b) presents the high resolution Si 2p spectra showing a single peak at binding energies of 103.6–103.7 eV while the O 1s spectra (Fig. 1(c)) showing a single peak at ~533.0 eV. This is consistent with the reported binding energies of Si 2p and O 1s for SiO_2 are 103.5 and 533.2 eV, respectively [43], therefore confirms the formation of SiO_2 from our process. In addition, the oxygen to silicon ratio of 2.3 is also indicative of the formation of SiO_2. A few factors could contribute to the excessive amount of oxygen: (1) according to the CasaXPS manual 2.3.15 Rev 1.2 [44] and other reported work [45,46], XPS atomic composition measurement has a scatter/error of about 10%; (2) the excessive amount of oxygen was likely to include a small amount of oxygen bound to carbon, possibly picked up during the sample transfer in air, and (3) the coating may also contain OH^- groups and other low molecular weight alkyl silicate oligomers. It ought to be noted that these OH^- groups, once formed, are difficult to remove [47] and may adversely affect battery performance because of its reactivity towards lithium metal [48]. Systematic and in-depth investigation need to be conducted in further research.

Fig. 2 shows coating gains vs number of coating/dipping times. The coating weight percentage gain demonstrates a linear relationship with the number of dips in the solution. In other words, every single dip provides a consistent amount of coating. This is a fluid dynamics phenomena which can be understood by introducing the dip coating thickness equation [49]:

$$h = \frac{0.94(\nu U_0)^{2/3}}{\gamma^{1/6}(\rho g)^{1/2}} \quad (3)$$

where h is coating film thickness, η is solution viscosity, U_0 is substrate withdraw speed, γ is liquid–vapour interface tension, ρ is solution density, g is acceleration of gravity. For a given solution, η, γ, ρ and g are constants. The coating film thickness is then solely determined by the substrate withdraw speed. If the speed was kept a constant during dipping, a consistent gain of coating can be obtained. In our experiments, the withdraw speed was kept at about 4 cm s^{-1}. In order to provide a visual understanding of the coating thickness, Fig. 3 presents two examples of SEM cross section analysis of the coated samples corresponding to the minimum (one dip, Fig. 3(a)) and the maximum (six dips, Fig. 3(b)) coating thickness, showing a coating thickness of about 1 and 6 μm, respectively.

The top surface SEM images of the uncoated PP separator and the coated separators are shown in Fig. 4. In contrast to the uncoated PP separator (Fig. 4(a)), close-packed SiO_2 nanoparticles interconnected by PVdF-HFP binder are present on the separator surface (Fig. 4(b–g)) comprising ceramic coating layers with various coating weight gains. The overall morphology of the SiO_2 coating layers

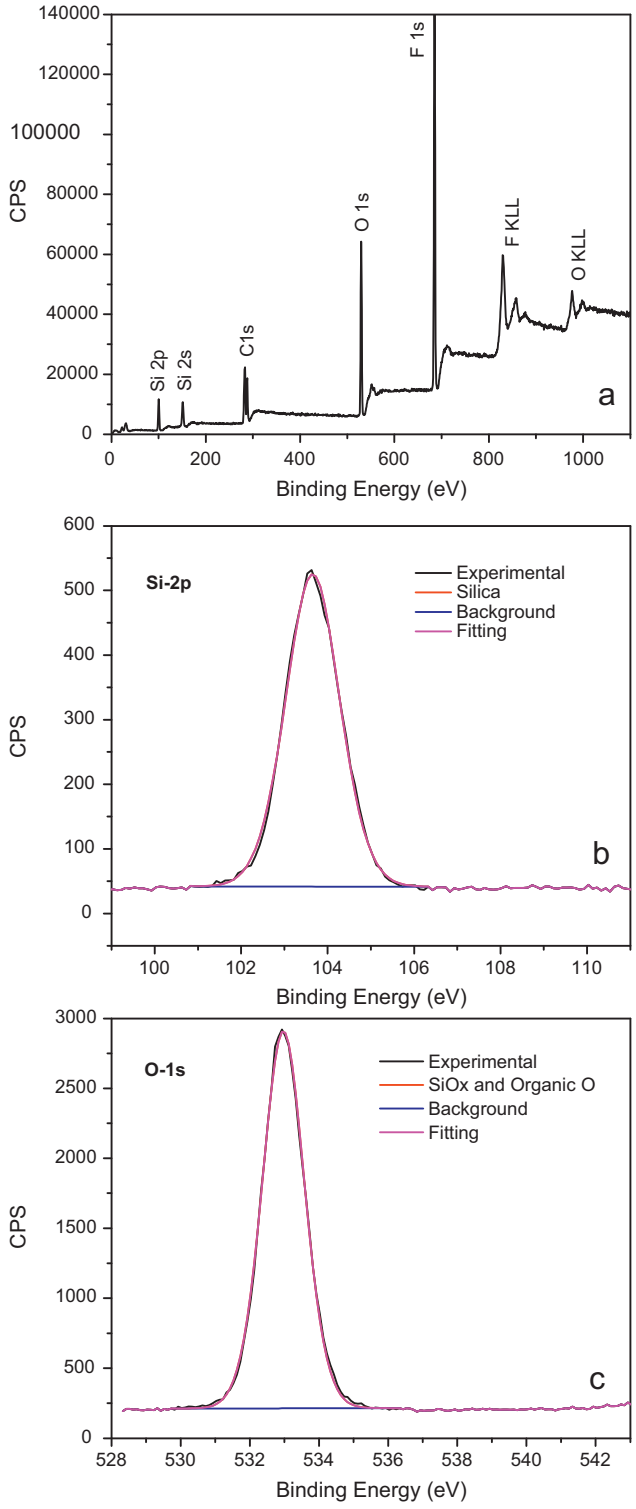

Fig. 1. XPS spectra of SiO_2 coated separator. (a) XPS survey spectrum; (b) the high-resolution Si-2p spectrum; (c) the high-resolution O-1s spectrum.

is similar to the nanoparticle arrangement driven by self-assembly (the spontaneous organization of materials through noncovalent interactions with no external intervention [50]), as was reported by Masuda et al. [51,52]. The morphology of the separator with the highest amount of coating (Fig. 4(g)) is different when compared with the other samples in that the surface is mostly covered with PVdF-HFP which forms a network of binder. Nano-sized particles exist within the binder network, as is clearly shown in the two

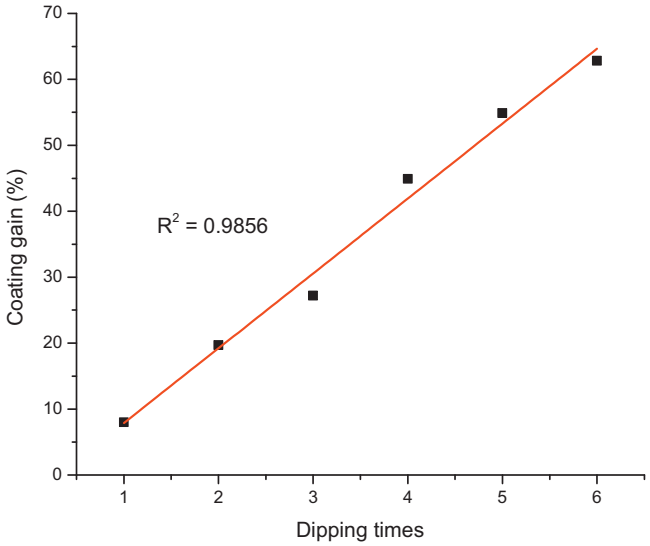

Fig. 2. Coating gain vs dipping times.

bird-nest-like insets in Fig. 4(g). The excessive binder build up is probably caused by the accumulation of the PVdF-HFP binder with repeated dipping, which results in the formation of an obvious network during drying process due to the viscose nature of the binder and the surface tension.

Understanding the coating composition is important, though a reliable direct measurement is difficult. However, acetone and ammonium water are highly volatile with a boiling temperature of 56.5 and 37.7 °C, respectively. TEOS is also categorized as a volatile organic compound (VOC) with a boiling point of 166–169 °C, much below the VOC high limit temperature of 250 °C under an atmospheric pressure of 101.3 kPa. With that, any of these residuals would evaporate during drying of the coating, particularly with the large surface area due to the porous nature of the coating. With that, the coating consists mainly of SiO_2 particle and PVdF-HFP binder. Given that a direct and quantitative measurement of the SiO_2/PVdF-HFP ratio in the coating is difficult, an indirect measurement was carried out by centrifuging the original deposition bath at 3500 rpm for one hour. Because the coating bath forms SiO_2 homogeneously and that the particles formed were observed to suspend uniformly for an extended period of time of several hours, it is reasonable to believe the ratio of two constituents in the coating and in the bath are consistent. This is particularly the case given that the bath was thoroughly agitated every time prior to the deposition of coating. The particles collected were then washed and centrifuged using fresh acetone for three times to clean the particles before drying. The dried particles were then weighed and compared with

Table 1
Specific surface area, pore diameter, pore volume with various coating gain.

Coating gain %	Specific surface area ($m^2\ g^{-1}$)	Pore size (nm)	Pore volume ($cm^3\ g^{-1}$)
0	54.0	27.5	0.47
8	53.7	25.5	0.35
20	50.1	19.1	0.29
27	50.0	22.3	0.28
45	52.2	22.0	0.31
55	58.5	22.0	0.34
63	49.8	24.9	0.33

the initial weight of PVdF-HFP binder added into the bath. From our measurement, the coating composition in terms of the weight ratio of SiO_2 to PVdF-HFP is 1.6–1.

Regarding porosity retention after coating, the specific surface areas, pore sizes and pore volumes were examined and listed in Table 1. As can be seen from Table 1, the specific surface areas and pore sizes are not changed significantly after coating as compared with plain separator. However, for the pore volumes, although it is not significantly different among the coated separators with various coating gains, the pore volumes decline approximately 30% for the coated separators from 0.47 $cm^3\ g^{-1}$ to an average of about 0.32 $cm^3\ g^{-1}$.

The wettability of the separator used in the lithium batteries plays a critical role in the battery performance because the separator with good wettability can effectively retain the electrolyte and facilitate its diffusion well into the cell assembly [7,8]. Contact angle (θ) measurement is one of the important indicators for wettability: the lower the contact angle the more wettable (hydrophilic) the surface is. However, it ought to be clarified that on a rough surface, the contact angle measurement is affected by the surface roughness even when the surface chemical composition is identical for a smooth and a rough surface [53]. When the surface is roughened, the apparent contact angle (θ_{app}) can be altered by a geometric factor, given by Wenzel's equation [54]:

$$\cos\ \theta_{app} = r\ \cos\ \theta \tag{4}$$

where r is a ratio of true surface area to the horizontal projection of surface area.

From Table 1, the separators with or without coating have similar pore size and specific surface area. These results indicate a similar roughness on the surface of separators before and after coating. As such, the r values in Eq. (4) are similar for different separators, and we can therefore directly use the apparent contact angle (θ_{app}) instead of contact angle (θ) for relative comparison of wettability of the separators. As shown in Table 2, the contact angle decreases from 38° to 30° for uncoated surface and a single dip coated surface, respectively due to the formation of hydrophilic SiO_2 particles. With further increase of coating thickness, the

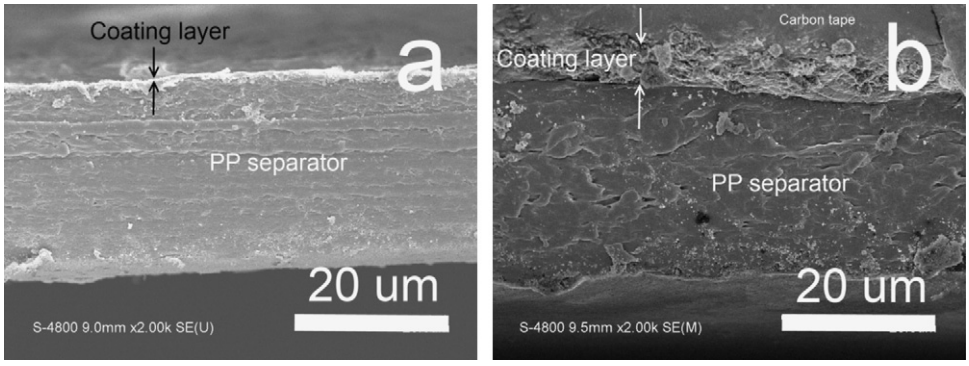

Fig. 3. SEM cross section analysis of coated samples: (a) one dip; (b) six dips.

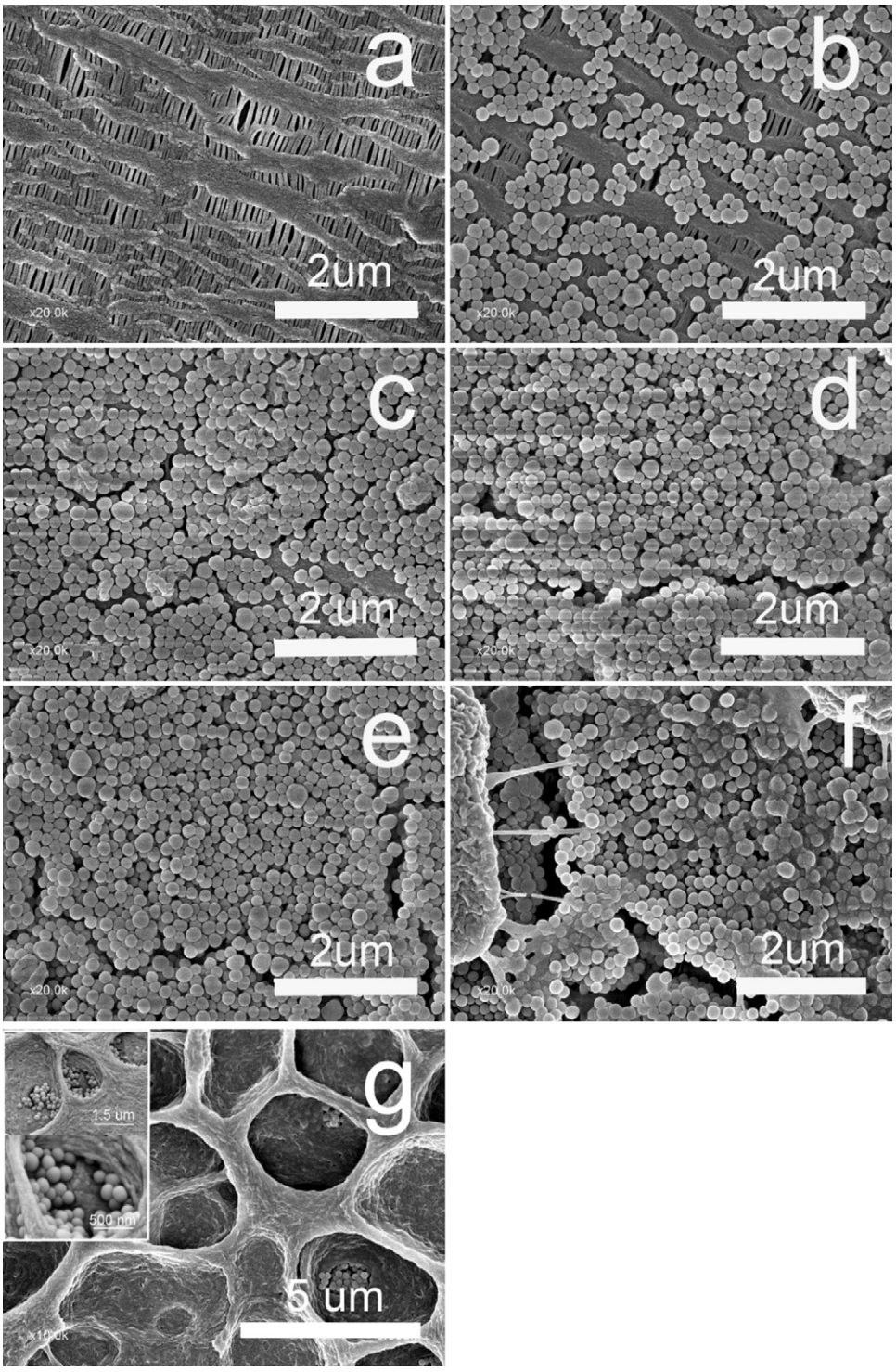

Fig. 4. SEM images of separator surface with and without SiO_2 particles coating. (a) Without coating, (b) 8%, (c) 20%, (d) 27%, (e) 45%, (f) 55%, and (g) 63% coating gain.

contact angle drastically reduced to below the measurement limit of the Kenco system which is below 10°. Such a low contact angle represents an excellent wettability of the coated surface. The relatively higher contact angle of the single dip coated surface could indicate that the separator surface was not entirely covered. In summary, all the contact angles of the coated separators as compared to the uncoated separator surface are consistently reduced which clearly demonstrates that coating improved the wettability of the separator surface.

Fig. 5 shows the electrolyte uptake as a function of coating gain. As was aforementioned, the hydrophilic SiO_2 particles in the coating improve the wettability thereby enhancing the electrolyte retention in the separators. For the uncoated PP membrane, the electrolyte filled into the pores and the electrolyte uptake was proportional to the separator porosity, i.e. the porosity of the separator acts as the only avenue for electrolyte uptake. In the case of SiO_2 particles coated separators, however, liquid electrolyte was not only trapped in the pores but also retained inside the porous

Table 2
Contact angles of 1 M $LiPF_6$ in DMC/EC (1:1 in volume) on uncoated separator and separators coated with various weight gain.

Coating gain (%)	Contact angles (°)
0	38
8	30
20	<10[a]
27	<10[a]
45	<10[a]
55	<10[a]
63	<10[a]

[a] The contact angle meter from Kernco Instruments has a measurement range of 10–120° with a low limit of 10°.

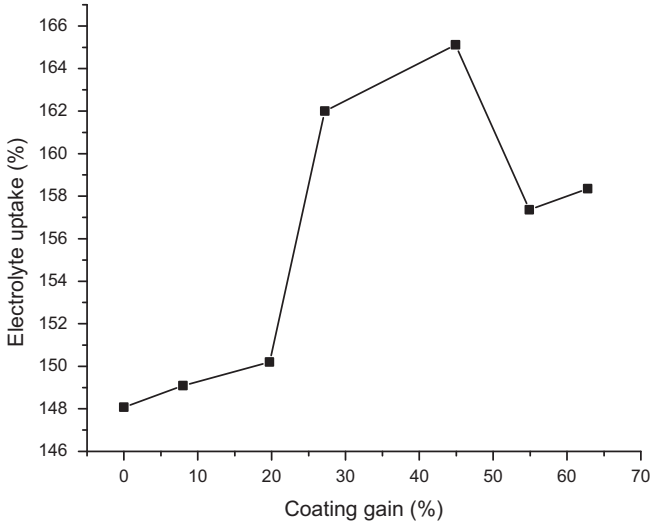

Fig. 5. Electrolyte uptake (%) of separators with various coating gain.

coating comprised of the hydrophilic SiO_2 particles and the PVdF-HFP network.

The separator must be mechanically strong to withstand high tension during the battery assembly and to resist the protrusion of the dendritic crystals formed during cell cycling. Fig. 6 shows the load (maximum) of the separators with and without coating. Despite non-negligible standard deviations, a general trend of increasing strength of the separators with increasing coating gain could be observed. Compared to the uncoated separator, the load (maximum) increased by ~10% at 8% coating gain and continues

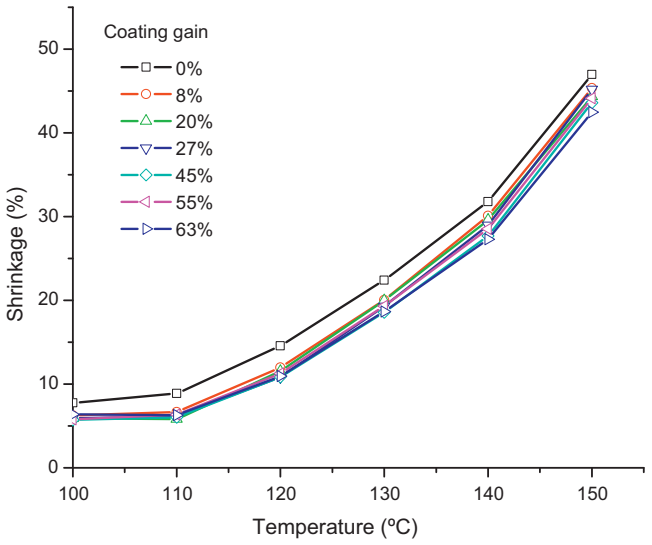

Fig. 7. Thermal shrinkage (%) at various temperatures and with different coating gain.

with further increase of coating. It is believed that SiO_2 particles and polymer chains in PVdF-HFP interact with each other by van der Waals force, etc., thus forming cross-linked porous structures and restricting the motion of molecular chains [55].

Thermal shrinkage of separators is another important issue pertaining to not only battery performance but also safety. A severely shrunk separator caused by the heat generated during cell cycling, particularly under high power output conditions such as for electric vehicles applications, could result in shorting of the electrodes along the perimeter of the separator. The ceramic coating layers are expected to prevent the separators from thermal shrinkage, due to the existence of the heat-resistant SiO_2 nanoparticles. Accordingly, the thermal shrinkage of the coated and uncoated separators was observed by measuring the dimensional change (area-based) after the separator was subjected to heat treatment at various temperatures for 0.5 h. Fig. 7 shows that all the SiO_2 coated separators have a reduced thermal shrinkage than the uncoated PP separator over a wider range of temperatures, which verifies that the introduction of ceramic coating layers is effective in improving the thermal performance of separators [21]. In addition, the thermal shrinkage of the coated separators was further examined as a function of coating thickness. At relatively low temperatures, the thermal shrinkage

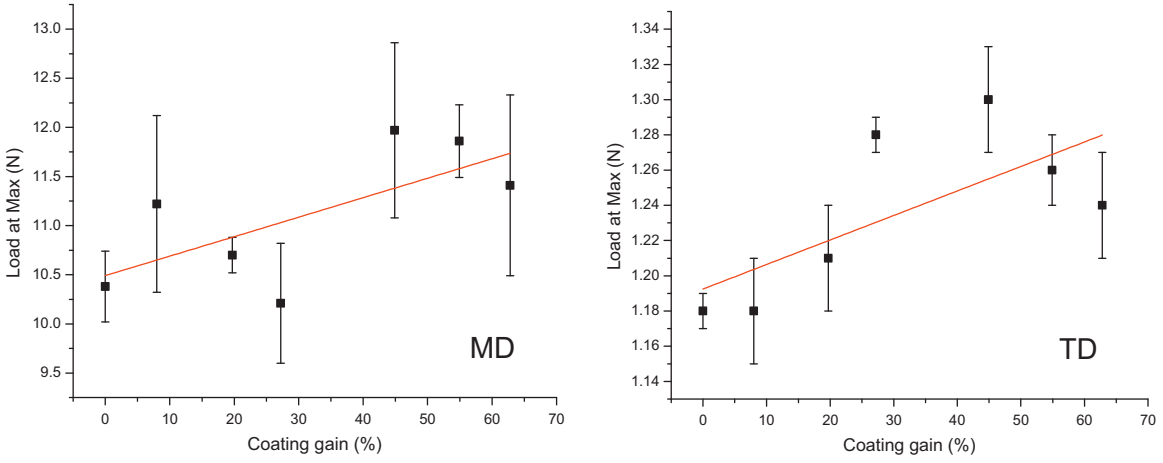

Fig. 6. Load (max) with various coating gains. MD and TD are machine direction and transverse direction.

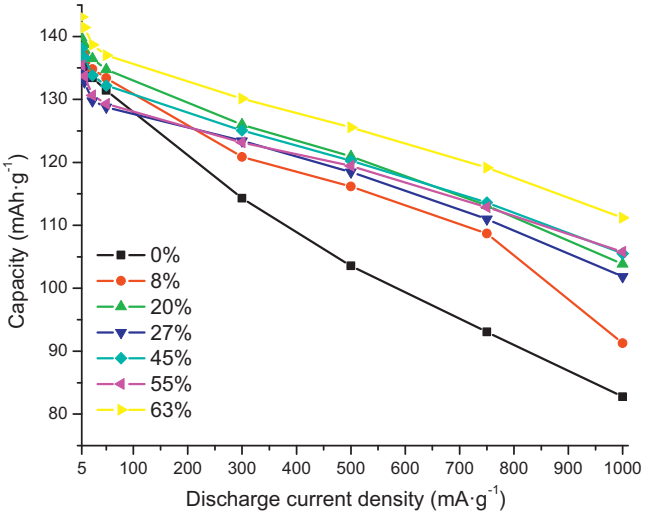

Fig. 8. Discharge capacity of separators with different coating gain at various discharge rates. The charging was conducted at 5 mA g^{-1}.

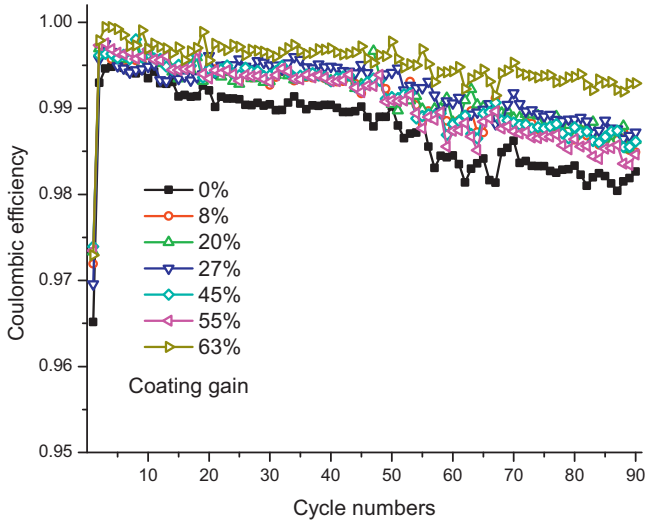

Fig. 9. Coulombic efficiency of separators with different coating gain at a charge/discharge rate of 50/50 mA g^{-1}.

for samples with different coating thickness does not exhibit significant change. However, at further elevated temperatures, the benefit of coating on thermal shrinkage becomes more pronounced with the increase of coating thickness. This improvement in the thermal shrinkage of the coated separators is attributed to the presence of a large amount of heat resistant SiO_2 nanoparticles in the ceramic coating layer [26] (coefficient of thermal expansion: PP $-8–10 \times 10^{-4}\,^{\circ}C^{-1}$ [56], SiO_2 $5 \times 10^{-7}\,^{\circ}C^{-1}$ [57]).

In addition, sufficient adhesion is always an important consideration in coating development. Unfortunately, the separator is a porous membrane of only 25 μm thick. It is soft, flexible, and stretchy, which makes a reliable quantitative measurement of bonding strength extremely challenging, if at all possible. However, to have some understanding about the coating adhesion, we conducted a basic scotch tape test to see if any particles can be peeled off from the separator. Repeated tests were carried out and no separation of the coating was observed. In addition, particles could fall off when subjected to heating and cooling, but no particles were observed to separate from the substrate when subjected to the thermal shrinkage test described above within a temperature range from room temperature to 150 °C. This temperature is significantly higher than the normal operating temperature of a Li battery. In addition, adhesion is mostly a concern when tensile force is applied to a coating. That is why a compressive internal stress is preferred and a tensile internal stress is avoided in coating development when attempting to achieve a high adhesion. In the case of Li battery assembling, the separator is sandwiched between the electrodes with stainless steel spring washers outside of each electrode. This puts the separator in a compressed state, namely, a compressive force is applied as opposed to a tensile force. The Scotch Tape and the thermal cycling test described above along with the compressed state the separator exists in a battery assembly suggest that adhesion is not expected to be a concern in our work. This proves that the binder (PVdF-HFP) effectively forms a gel network during the deposition and firmly binds the particles inside the gel matrix and on to the substrate surface.

Fig. 8 shows the discharge capacity at different discharge rates for batteries fabricated using uncoated separator and separators coated of various thicknesses. All the charging was conducted at 5 mA g^{-1}. As can be clearly seen, all the coated separators consistently resulted in an increase in battery capacity as compared to the battery using uncoated separator. In addition, this increase becomes more significant with an increasing rate of discharge. This clearly shows a much improved rate capability of batteries using SiO_2 coated separators. An improved rate capability after Al_2O_3 coating was reported by Choi et al. [24]. The improved rate performance was ascribed to the favourable interfacial charge transport between the electrodes and the electrolytes in the cell, because the coating layer on both sides of the separator was able to assist in the adhering of separator to the electrodes after soaking in the electrolyte solution. It should be stressed that this observation is not well understood because coating is expected to block the original pores in the separator. While Choi's explanation might also be true in our case, we cannot rule out the possibilities of other effects. An example of these possibilities is related to the wetting mechanism of the separators. The uncoated separator has poor wettability with a contact angle of 38° while all the coatings with more than one dip show a much improved wettability represented by the very low contact angles even below the detection limit of 10°. Even though coating reduced the porosity, the drastically improved wettability indicates a significantly increased adhesive force at the electrolyte/separator interface, including the inner surface of the pores. This increased adhesive force of the coated separators vs the cohesive force within the electrolyte species (molecules and ions) therefore enhances the transport of these species. In addition, all the species have much smaller radius (Li^+ of 0.09–0.109 nm, PF_6^- of 0.16 nm, EC molecular of 0.25 nm, and DEC molecular of 0.30 nm) as compared to the pore size of the separator on a micron meter scale. This enhanced transport of species in the electrolyte suggests a reduction of ion/molecule transport impedance as reported by others [24,26]. This reduced impedance could then facilitate the kinetics of charge/discharge reactions, resulting in an improved rate performance particularly at higher rates. While the beneficial effect of SiO_2 coating on the rate capability of battery is shown based on our deposition method and our experimental results, more systematic studies will be systematically carried out for further understanding.

Fig. 9 shows the Coulombic efficiency of separators with various coating gains as a function of charge/discharge cycle numbers. The cells were cycled at 10 mA g^{-1} for 10 cycles followed by 90 cycles at 50 mA g^{-1} between the voltages of 2.5 and 4.2. The Coulombic efficiency is defined as the ratio of the discharge capacity to charge capacity. During the first cycle, the Coulombic efficiency is relatively low. One of the main reasons is that the Coulombic efficiency is associated with the irreversible capacity loss during the first cycle that involves electrolyte decomposition and subsequent

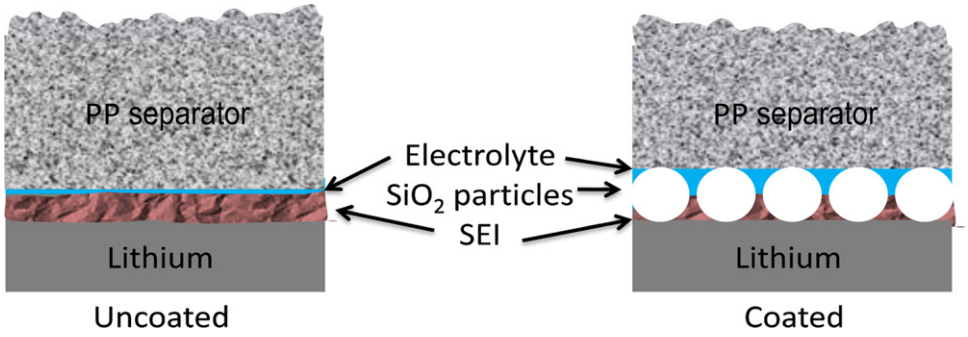

Fig. 10. Schematic of SEI formation on uncoated and coated PP separator.

formation of a surface film (solid electrolyte interphase or interface: SEI) on the electrodes [58,59]. The surface film is conductive for lithium ions but is insulating electronically, which prevents the electrodes interaction with non-aqueous organic solutions. Some lithium ions are consumed by the formation of SEI and therefore not contributing to the charge/discharge cycling, resulting in a loss of Coulombic efficiency during the first cycle [60]. However, as can be seen from Fig. 9, the Coulombic efficiency of all the 6 coated separators is higher than the plain separator. This might be related to a more efficient SEI formation. For example, when the coated separator is in close contact with the electrode surface, the SEI film could now be formed during the first cycle as a composite film consisting of lithium salt(s) that fill in the porous structure of SiO_2 coating, as opposed to the conventional SEI film of only lithium salt(s), see the schematic illustration in Fig. 10. This insulating film starts with an already insulating layer of SiO_2 particles, thus requiring only a portion of the lithium ions consumed to form an SEI without SiO_2 particles. As such, more lithium ions are reserved for charge/discharge cycling thereby increasing the cell Coulombic efficiency. After the first cycle in our work, or the first several cycles in other reported cases, the reserved amount of lithium ions continue to be available for maintaining a higher efficiency of the cells using coated separators for extended cycles. While this is a new model trying to explain the phenomenon of cell 'activation' during the first or early cycles of lithium-ion cells, more research is required to further verify or confirm the model. Other possibilities for the Coulombic efficiency increase could include improved electrochemical kinetics because of the enhanced electrolyte update and surface wettability of the separators with SiO_2 coating.

4. Conclusions

A new separator was successfully developed by depositing SiO_2 ceramic layers of nanoparticles onto the PP separators for lithium-ion battery using a simple yet effective SiO_2 formation and deposition process. The existence of the heat-resistant and hydrophilic SiO_2 coating layers resulted in not only a substantial reduction in the thermal shrinkage, but also enhancement in tensile strength and improvement in surface wettability, electrolyte uptake and cell performances as compared to the plain PP separator. The much improved battery rate capability and higher Coulombic efficiency represent better electrochemical cell performance suitable particularly for high power applications, while the increased mechanical strength and reduced thermal shrinkage translate into enhanced battery safety. This new technology is simple, cost effective, and can be easily commercialized as a roll-to-roll production on a large scale. In addition, the formation of a possible composite SEI film could explain the higher Coulombic efficiency, though further investigation will need to be conducted.

Acknowledgement

The authors are grateful to the financial support provided by the Electric Mobility Program of PERD, Natural Resources Canada.

References

[1] M. Armand, J.M. Tarascon, Nature 451 (2008) 652–657.
[2] D. Linden, T.B. Reddy, Handbook of Batteries, 3rd ed., McGraw-Hill, New York, 2002.
[3] F. Croce, G.B. Appetecchi, L. Persi, B. Scrosati, Nature 394 (1998) 456–458.
[4] G. Venugopal, J. Moore, J. Howard, S. Pendalwar, Journal of Power Sources 77 (1999) 34–41.
[5] B.L. Luan, G. Campbell, M. Gauthier, X.Y. Liu, I. Davidson, J. Nagata, M. Lepinay, F. Bernier, S. Argue, ECS Transactions 25 (2010) 59–71.
[6] R.J. Brodd, H.M. Friend, J.C. Nardi, Lithium ion Battery Technology, ITE-JEC Press, 1995.
[7] S.S. Zhang, Journal of Power Sources 164 (2007) 351–364.
[8] P. Arora, Z.M. Zhang, Chemical Reviews 104 (2004) 4419–4462.
[9] C.T. Love, Journal of Power Sources 196 (2011) 2905–2912.
[10] C.M. López, J.T. Vaughey, D.W. Dees, Journal of the Electrochemical Society 156 (2009) A726–A729.
[11] X.W. Zhang, Y. Li, S.A. Khan, P.S. Fedkiw, Journal of the Electrochemical Society 151 (2004) A1257–A1263.
[12] E. Eweka, J.R. Owen, A. Ritchie, Journal of Power Sources 65 (1997) 247–251.
[13] H.S. Jeong, J.H. Kim, S.Y. Lee, Journal of Materials Chemistry 20 (2010) 9180–9186.
[14] T.H. Cho, M. Tanaka, H. Onishi, Y. Kondo, T. Nakamura, H. Yamazaki, S. Tanase, T. Sakai, Journal of Power Sources 181 (2008) 155–160.
[15] Y. Lee Min, J.W. Kim, N.S. Choi, J. Lee An, W.H. Seol, J.K. Park, Journal of Power Sources 139 (2005) 235–241.
[16] M. Tanaka, T.H. Cho, T. Nakamura, T. Tarao, M. Kawabe, T. Sakai, Electrochemistry 78 (2010) 982–987.
[17] Y. Liang, L. Ji, B. Guo, Z. Lin, Y. Yao, Y. Li, M. Alcoutlabi, Y. Qiu, X. Zhang, Journal of Power Sources 196 (2011) 436–441.
[18] T.H. Cho, M. Tanaka, H. Ohnishi, Y. Kondo, M. Yoshikazu, T. Nakamura, T. Sakai, Journal of Power Sources 195 (2010) 4272–4277.
[19] J.H. Park, J.H. Cho, W. Park, D. Ryoo, S.J. Yoon, J.H. Kim, Y.U. Jeong, S.Y. Lee, Journal of Power Sources 195 (2010) 8306–8310.
[20] H.S. Jeong, S.C. Hong, S.Y. Lee, Journal of Membrane Science 364 (2010) 177–182.
[21] H.S. Jeong, D.W. Kim, Y.U. Jeong, S.Y. Lee, Journal of Power Sources 195 (2010) 6116–6121.
[22] H.S. Jeong, J.H. Noh, C.G. Hwang, S.H. Kim, S.Y. Lee, Macromolecular Chemistry and Physics 211 (2010) 420–425.
[23] Y.S. Chung, S.H. Yoo, C.K. Kim, Industrial and Engineering Chemistry Research 48 (2009) 4346–4351.
[24] J.A. Choi, S.H. Kim, D.W. Kim, Journal of Power Sources 195 (2010) 6192–6196.
[25] M. Kim, G.Y. Han, K.J. Yoon, J.H. Park, Journal of Power Sources 195 (2010) 8302–8305.
[26] H.S. Jeong, S.Y. Lee, Journal of Power Sources 196 (2011) 6716–6722.
[27] J.C. Su, S.Y. Liang, W.L. Liu, T.C. Jan, Journal of Manufacturing Science and Engineering-Transactions of the ASME 126 (2004) 779–786.
[28] W. Stöber, A. Fink, E. Bohn, Journal of Colloid and Interface Science 26 (1968) 62–69.
[29] H.A. Ketelson, R. Pelton, M.A. Brook, Langmuir 12 (1996) 1134–1140.
[30] D.L. Green, J.S. Lin, Y.F. Lam, M.Z.C. Hu, D.W. Schaefer, M.T. Harris, Journal of Colloid and Interface Science 266 (2003) 346–358.
[31] G.H. Bogush, C.F. Zukoski Iv, Journal of Colloid and Interface Science 142 (1991) 19–34.
[32] G.H. Bogush, C.F. Zukoski Iv, Journal of Colloid and Interface Science 142 (1991) 1–18.
[33] T. Matsoukas, E. Gulari, Journal of Colloid and Interface Science 132 (1989) 13–21.

[34] T. Matsoukas, E. Gulari, Journal of Colloid and Interface Science 124 (1988) 252–261.
[35] D.L. Green, S. Jayasundara, Y.F. Lam, M.T. Harris, Journal of Non-Crystalline Solids 315 (2003) 166–179.
[36] S. Sadasivan, A.K. Dubey, Y. Li, D.H. Rasmussen, Journal of Sol–Gel Science and Technology 12 (1998) 5–14.
[37] S.L. Chen, P. Dong, G.H. Yang, J.J. Yang, Industrial and Engineering Chemistry Research 35 (1996) 4487–4493.
[38] C.J. Brinker, G.W. Scherer, Sol–Gel Science, Academic Press, Boston, 1990.
[39] S.L. Chen, P. Dong, G.H. Yang, Journal of Colloid and Interface Science 189 (1997) 268–272.
[40] A. van Blaaderen, A.P.M. Kentgens, Journal of Non-Crystalline Solids 149 (1992) 161–178.
[41] A. Van Blaaderen, J. Van Geest, A. Vrij, Journal of Colloid and Interface Science 154 (1992) 481–501.
[42] X.D. Wang, Z.X. Shen, T. Sang, X.B. Cheng, M.F. Li, L.Y. Chen, Z.S. Wang, Journal of Colloid and Interface Science 341 (2010) 23–29.
[43] B.V. Crist, Handbook of Monochromatic XPS Spectra: Semiconductors, Wiley, 2000.
[44] N. Fairley, CasaXPS Manual 2.3.15 Rev 1.2, Casa Software Ltd., 2009.
[45] G. Friedbacher, H. Bubert, Surface and Thin Film Analysis: A Compendium of Principles, Instrumentation, and Applications, John Wiley & Sons, 2011.
[46] G.P. Lopez, D.G. Castner, B.D. Ratner, Surface and Interface Analysis 17 (1991) 267–272.
[47] J.M. Kim, S.M. Chang, S.M. Kong, K.-S. Kim, J. Kim, W.-S. Kim, Ceramics International 35 (2009) 1015–1019.
[48] F. Tran-Van, M. Provencher, Y. Choquette, D. Delabouglise, Electrochimica Acta 44 (1999) 2789–2792.
[49] C.J. Brinker, G.C. Frye, A.J. Hurd, C.S. Ashley, Thin Solid Films 201 (1991) 97–108.
[50] C.J. Brinker, Y. Lu, A. Sellinger, H. Fan, Advanced Materials 11 (1999) 579–585.
[51] Y. Masuda, T. Itoh, K. Koumoto, Langmuir 21 (2005) 4478–4481.
[52] Y. Masuda, M. Itoh, T. Yonezawa, K. Koumoto, Langmuir 18 (2002) 4155–4159.
[53] B. Luan, M. Yeung, W. Wells, X. Liu, Applied Surface Science 156 (2000) 26–38.
[54] R.N. Wenzel, Industrial & Engineering Chemistry 28 (1936) 988–994.
[55] Y. Zhang, G. Zhang, T. Du, L. Zhang, Electrochimica Acta 55 (2010) 5793–5797.
[56] F. Rodriguez (Ed.), Principles of Polymer Systems, 3rd ed., Hemisphere Pub. Corp., New York, 1989.
[57] S. Franssila (Ed.), Introduction to Microfabrication, 2nd ed., John Wiley & Sons, 2010.
[58] J.O. Besenhard, Handbook of Battery Materials, Wiley-VCH, 1999.
[59] T. Nakajima, Journal of Fluorine Chemistry 128 (2007) 277–284.
[60] Z. Ogumi, S.K. Jeong, Electrochemistry 71 (2003) 1011–1017.